Published in final edited form as:
Science. 2020 June 19; 368(6497): 1371–1376. doi:10.1126/science.aax0860.

Immunometabolic T cell failure induces multimorbidity and aging

Gabriela Desdín-Micó[1,2], **Gonzalo Soto-Heredero**[1,2,†], **Juan Francisco Aranda**[1,2,†], **Jorge Oller**[1,2,†], **Elisa Carrasco**[1,2], **Enrique Gabandé-Rodríguez**[1,2], **Eva Maria Blanco**[1,2], **Arantzazu Alfranca**[3], **Lorena Cusso**[4,5], **Manuel Desco**[4,5], **Borja Ibañez**[5,6,7], **Arancha R. Gortazar**[8], **Pablo Fernández-Marcos**[9], **Maria N. Navarro**[2,3], **Bruno Hernaez**[2], **Antonio Alcamí**[2], **Francesc Baixauli**[10,¶], **María Mittelbrunn**[1,2,¶,*]

[1]Institute de Investigación Sanitaria Hospital 12 de Octubre (imas12), Madrid, Spain

[2]Departamento de Biología Molecular, Centro de Biología Molecular Severo Ochoa (CBMSO), Consejo Superior de Investigaciones Científicas (CSIC)-Universidad Autónoma de Madrid (UAM), Madrid, Spain

[3]Hospital Universitario de la Princesa, Madrid, Spain

[4]Departamento de Bioingeniería e Ingeniería Aeroespacial, Universidad Carlos III de Madrid, Instituto de Investigación Sanitaria Gregorio Marañón; Centro de Investigación Biomédica en Red de Salud Mental (CIBERSAM), Spain

[5]Centro Nacional de Investigaciones Cardiovasculares (CNIC), Madrid, Spain

[6]IIS-Fundación Jiménez Díaz, Madrid, Spain

[7]CIBERCV, Madrid, Spain, Madrid, Spain

[8]Bone Physiopathology Laboratory, Applied Molecular Medicine Institute (IMMA), Universidad San Pablo-CEU, Madrid, Spain

[9]Metabolic Syndrome Group - BIOPROMET, Madrid Institute for Advanced Studies - IMDEA Food, CEI UAM+CSIC, Madrid, Spain

[10]Department of Immunometabolism, Max Planck Institute of Immunobiology and Epigenetics, Freiburg, Germany

Abstract

The impact of immunometabolism on age-associated diseases remains uncertain. Here, we show that T cells with dysfunctional mitochondria act as aging accelerators. They instigate

*Correspondence to: mmittelbrunn@cbm.csic.es .
†for equal contributions
¶for equal contributions

Author contributions

G.D-M, G.S-H, J.F.A, J.O, E.C, E.G-R, M.N, L.C, F.B, E.M.B, and B.H. performed experimental work and analyzed the data. B.I, A. Alfranca, M.D. and A. Alcami provided technical and scientific support. F.B. and M.M. designed the research. G.D-M and M.M. wrote the manuscript. G.S-H, J.F.A. and J.O. contributed equally to this study. F.B. and M.M. contributed equally to this study.

Competing interests

The authors declare no competing interests.

Europe PMC Funders Author Manuscripts

multiple age-related features, including metabolic, cognitive, physical and cardiovascular alterations, which together result in premature death. Metabolic failure in T cells induces the accumulation of circulating cytokines, resembling the chronic inflammation that characterizes aging ("inflammaging"). We also present evidence that this cytokine storm is a systemic inducer of senescence. Dampening inflammation by blocking TNF-α signaling or preventing senescence with NAD^+ precursors partially rescue premature aging in mice with metabolically defective T cells. Thus, T cells have the capacity to regulate organismal fitness and lifespan, highlighting the importance of tight immunometabolic control in both aging and the onset of age-associated diseases.

The emerging field of immunometabolism (1–5) is opening up therapeutic opportunities for the treatment not only of inflammatory and autoimmune disorders (6), but also of metabolic diseases and cancer (7–10). However, the utility of targeting immunometabolism to prevent the onset of age-associated diseases and multimorbidity has not been previously addressed.

An age-related decline in mitochondrial function has been observed in various cells and tissues, including T cells (11). To investigate the consequences of T cell metabolic decline in healthy aging, we used *Tfam*$^{fl/fl}$ *Cd4*^{Cre} mice. *Tfam* is a nuclear gene encoding mitochondrial transcription factor A (TFAM), which both stabilizes mtDNA and initiates mtDNA replication (12). In *Tfam*$^{fl/fl}$ *Cd4*^{Cre} mice, Tfam is depleted in both CD4 and CD8 T lymphocytes (13). Lack of Tfam in T cells reduced the numbers of total circulating CD4 and CD8 T cells (fig. S1A). Tfam depletion induced a sharp decrease in their mtDNA content (fig. S1B) and the loss of expression of key electron transport chain components, forcing a metabolic reprogramming towards glycolysis (13) (Fig. 1A-C). T cells from young (2 months old) *Tfam*$^{fl/fl}$ *Cd4*^{Cre} mice recapitulated features of the mitochondrial dysfunction that appears in aged (22 months old) wild-type mice (Fig. 1A-C). This mitochondrial decline was associated with Th1 cell skewing, characterized by higher secretion of inflammatory type 1 cytokines IFN-γ and TNF-α, and the increased expression of the Th1 cell master regulator T-bet (Fig. 1D-E, fig. S1C). In addition to this pro-inflammatory phenotype, young (2 months old) *Tfam*$^{fl/fl}$ *Cd4*^{Cre} mice were immunocompromised to a similar extent as old (22 months old) wild-types. We infected *Tfam*$^{fl/fl}$ *Cd4*^{Cre} mice with ectromelia virus (ECTV), a highly virulent mouse poxvirus that causes a disease similar to human smallpox, and compared them with young or old control mice. Infection with ECTV killed old wild type mice and young *Tfam*$^{fl/fl}$ *Cd4*^{Cre} mice in the first 10 days of infection, whereas all young controls were able to survive this acute infection (Fig. 1F). Thus, *Tfam*-deficient T cells recapitulate metabolic, phenotypic and functional features of aged T cells. We observed that *Tfam*$^{fl/fl}$ *Cd4*^{Cre} mice presented premature inflammaging, with 7-month-old *Tfam*$^{fl/fl}$ *Cd4*^{Cre} mice having similar serum levels of the inflammaging-associated cytokines IL-6, IFN-γ, and TNF-α to 22-month-old wild types (Fig. 1G, fig. S1D-E). In humans, inflammaging predicts susceptibility to cardiovascular diseases, neurodegeneration, frailty, and multimorbidity (14–16). *Tfam*$^{fl/fl}$ *Cd4*^{Cre} mice displayed a premature aged appearance from the age of 7 months (Fig. 1H) and developed anemia, kyphosis, and low body weight (Fig. 1I-K, fig. S1F). An additional indicator of aging in *Tfam*$^{fl/fl}$ *Cd4*^{Cre} mice was a significant thinning of hypodermal fat (Fig. 1L). Consistent with a premature aging phenotype, metabolic cage experiments revealed that *Tfam*$^{fl/fl}$ *Cd4*^{Cre} mice were less

active and slower than controls, despite higher energy expenditure (Fig. 1M, fig. S1G). Importantly, mean lifespan in *Tfam*$^{fl/fl}$ *Cd4*^{Cre} mice was half that of controls (483 days versus 984 days) (Fig. 1N). Although Tfam deletion in regulatory T cells induces lethal autoimmunity (17), *Tfam*$^{fl/fl}$ *Cd4*^{Cre} mice showed no differences in the level of serum autoantibodies (fig. S1H).

To evaluate the potential of *Tfam*$^{fl/fl}$ *Cd4*^{Cre} mice as a model of age-related multimorbidity, we analyzed muscular, cardiovascular, and cognitive fitness. Histological analyses of *Tfam*$^{fl/fl}$ *Cd4*^{Cre} muscle revealed a reduced fiber diameter (Fig. 2A). Imaging analysis of gastrocnemius muscle after injection of ^{18}F-fluorodeoxyglucose (^{18}F-FDG) revealed significantly lower glucose uptake in *Tfam*$^{fl/fl}$ *Cd4*^{Cre} mice (Fig. 2B). Lower skeletal muscle strength was confirmed by the grip strength test (Fig. 2C). Moreover, *Tfam*$^{fl/fl}$ *Cd4*^{Cre} muscle upregulated the expression of genes encoding the ubiquitin ligases MuRF-1 and Atrogin-1, as well as inflammatory markers (Fig. 2D, fig. S2A). *Tfam*$^{fl/fl}$ *Cd4*^{Cre} mice displayed a marked loss of gWAT mass, and smaller adipocytes (Fig. 2E,F). These differences were accompanied by elevated expression levels of the adipose triglyceride lipase (ATGL) and plasma levels of non-esterified fatty acids in *Tfam*$^{fl/fl}$ *Cd4*^{Cre}, indicating lipolysis induction (Fig. 2G,H). Thus, the loss of T cell immunometabolic control induces sarcopenia and lipolysis. *Tfam*$^{fl/fl}$ *Cd4*^{Cre} mice showed evidence of cardiac atrophy (Fig. 2I, fig. S2B). Histological and echocardiographic analysis revealed relative reduction in left ventricular thickness, reduced left ventricular diameter and volume, and smaller cardiomyocyte size (Fig. 2J, fig. S2C–F). These features were accompanied by a higher heart rate (Fig. 2K) and the induction of cardiac stress markers *Foxo3a* and *Nppa* (fig. S2G). *Tfam*$^{fl/fl}$ *Cd4*^{Cre} mice displayed diastolic failure characterized by reduced cardiac output, as well as elevated normalized lung weight together with signs of lung congestion on CT scan (Fig. 2L,M, and fig. S2H). Diastolic dysfunction was also evident from left ventricular (LV) relaxation defects detected in the mitral flow pattern (Fig. 2N). *Tfam*$^{fl/fl}$ *Cd4*^{Cre} mice developed an age-dependent aortic dilation (Fig. 2O) correlated with increased mRNA expression of inducible nitric oxide synthase (*Nos2*), decreased mRNA expression of the contractile markers as well as decreased blood pressure (Fig. 2P,Q). Consistent with these findings, 77% of *Tfam*$^{fl/fl}$ *Cd4*^{Cre} mice had aortic regurgitation, compared with 16% of controls. Histological analysis of the aortas allowed us to identify aortic dissections associated with inflammatory foci in 50% of *Tfam*$^{fl/fl}$ *Cd4*^{Cre} animals (fig. S2I). Thus *Tfam*$^{fl/fl}$ *Cd4*^{Cre} mice appear to develop cardiac atrophy and overt heart failure, and severe cardiovascular alterations, which can precipitate death. *Tfam*$^{fl/fl}$ *Cd4*^{Cre} mice also showed signs of neurological disability, including an influx of T cells in the fornix area of the brain and defects in motor coordination in both the rotarod and the tail suspension tests (Fig. 2R-T). Together, these data support a role for T cells beyond host defense (18, 19), and indicate that the metabolic fitness of T cells is critical for organismal homeostasis.

To verify whether this multimorbidity phenotype was due to a mitochondrial failure in T cells, we used an alternative to delete *Tfam* in T cells. We generated *Tfam*$^{fl/fl}$ *Lck*^{Cre} mice, in which Cre recombinase is expressed under the control of the lymphocyte protein tyrosine kinase (Lck) promoter. *Tfam*$^{fl/fl}$ *Lck*^{Cre} mice presented comparable metabolic and functional alterations in T cells, and similar premature age-associated multimorbidity to *Tfam*$^{fl/fl}$ *Cd4*^{Cre} mice (fig. S3). To identify the molecular mechanism by which T cell metabolic

failure drives organismal frailty and multimorbidity, we performed liver transcriptomics. *Tfam*$^{fl/fl}$ *Cd4*^{Cre} liver showed significant upregulation of genes associated with senescence (fig. S4A). One of the most upregulated transcripts related to senescence was *Cdkn1a*, which encodes the cyclin inhibitor p21 (q-value = 0.003) (Fig. 3A). *Tfam*$^{fl/fl}$ *Cd4*^{Cre} mice showed elevated protein levels of senescence markers p21$^{Waf/Cip1}$ and p53 in the liver. This elevation of p21 was also observed in the heart, gWAT, and pancreas (Fig. 3B). In addition, activity of senescence-associated β-galactosidase was higher in Tfam$^{fl/fl}$ Cd4^{Cre} gWAT and kidney than in controls (Fig. 3C,D, fig. S4B,C). Analysis of *Tfam*$^{fl/fl}$ *Lck*^{Cre} mice confirmed senescence induction in various tissues (fig. S3M).

Because in vitro incubation of cancer cells with the type 1 cytokines induces senescence (20), we hypothesized that the type 1 cytokines present in *Tfam*$^{fl/fl}$ *Cd4*^{Cre} mice drive systemic senescence. Incubation of mouse cells with *Tfam*$^{fl/fl}$ *Cd4*^{Cre} serum or TNF-α was sufficient to increase p21$^{Waf/Cip1}$ levels in hepatocytes, and pre-adipocytes, supporting the argument that inflammatory mediators induce senescence and premature aging (Fig. 3E, fig. S4D). To dissect the contribution of TNF-α to the multimorbidity phenotype, we treated *Tfam*$^{fl/fl}$ *Cd4*^{Cre} mice with the TNF-α inhibitor etanercept. Blocking TNF-α prevented systemic senescence (Fig. 3F,G) and muscle, cardiovascular and cognitive alterations (Fig. 3H-K). Bone marrow (BM) transplantation from *Tfam*$^{fl/fl}$ *Cd4*^{Cre} mice into T cell-deficient mice (*Cd3e*$^{-/-}$) (fig. S5A,B) recapitulated the type 1 cytokine storm observed in *Tfam*$^{fl/fl}$ *Cd4*^{Cre} mice (fig. S5C-E) and showed sings of senescence in multiple tissues (Fig. 3L-N). *Cd3e*$^{-/-}$ mice reconstituted with *Tfam*$^{fl/fl}$ *Cd4*^{Cre} BM, but not with control BM, developed a premature aged appearance after 16 weeks (fig. S5F), and reproduced the multimorbidity phenotype (fig. S5G-J). Thus, T cells with mitochondrial dysfunction are able to induce systemic senescence in peripheral tissues via type 1 cytokine storm.

Notably, the senescence observed in *Tfam*$^{fl/fl}$ *Cd4*^{Cre} mice was accompanied by a low NAD^+/NADH ratio in peripheral tissues (Fig. 4A, fig. S6A). This was consistent with the reported decline in NAD^+ levels during aging (21). NAD^+ is a metabolic cofactor with a critical role in mitochondrial function, and restoring NAD^+ levels confers protection against age-associated diseases (21–25). Recent data support that supplementation with the NAD^+ precursor nicotinamide riboside (NR) reduces inflammaging in the elderly (26). Accordingly, we observed that NR decreased the serum levels of TNF-α in aged mice (fig. S6B). To test whether NAD^+ boosting strategies could prevent tissue damage caused by inflammaging, we treated *Tfam*$^{fl/fl}$ *Cd4*^{Cre} mice with NR for 10 weeks to restore the NAD^+/NADH ratio (Fig. 4A,B). Although NR neither restored weight loss nor reversed the Th1 cell phenotype (Fig. 4C), it successfully reversed skeletal muscle wasting and anemia. Furthermore, most of the cardiovascular alterations found in *Tfam*$^{fl/fl}$ *Cd4*^{Cre} mice were also reversed (Fig. 4D-G). NR treatment also increased physical activity levels of *Tfam*$^{fl/fl}$ *Cd4*^{Cre} mice and reversed tissue senescence and inflammation (Fig. 4H-K, and fig. S6C). Finally, a principal component analysis of liver transcriptomics classified *Tfam*$^{fl/fl}$ *Cd4*^{Cre} mice treated with NR closer to controls than to untreated *Tfam*$^{fl/fl}$ *Cd4*^{Cre} mice (Fig. 4L). IPA analysis linked NR treatment to of pathways associated with lipid metabolism, inflammation, morbidity, and mortality (Fig. 4M and table S1). Thus, NR can reverse transcriptional changes related to aging in *Tfam*$^{fl/fl}$ *Cd4*^{Cre} mice.

With the continuous extension of life expectancy, there is an urgent need to understand the common molecular pathways by which aging results in a progressively higher susceptibility to diseases (27). Our results indicate that metabolic changes in the immune system promote age-related deterioration in other tissues, leading to multimorbidity and premature death. Dysregulated T cell metabolism triggers a type 1 cytokine storm that induces senescence in several tissues. Furthermore, we have used this novel model of multimorbidity and premature aging to test for drugs that can delay aging signs. We found that NAD^+ precursors can prevent tissue damage associated with sustained inflammation, supporting their potential for preventing age-associated multimorbidity. Whether targeting senescence or boosting NAD^+ levels would have beneficial effects beyond age-associated diseases in patients with cachexia or cytokine-release syndrome will require further investigation. Our results place immunometabolism at the crossroads of inflammation, senescence and aging, highlighting its potential as a therapeutic target for delaying aging and aging-associated diseases.

Supplementary Material

Refer to Web version on PubMed Central for supplementary material.

Acknowledgments

We thank N.G. Larsson for *Tfam*$^{fl/fl}$ mice, R. Tejedor and J.L de Pablos for technical support, and C. López-Otín, M. Serrano, and B. Alarcón for scientific discussion. We also thank A. de Francisco, Y. Sierra, and M. de la Jara Felipe for their excellent work with animal preparation and imaging protocols and D. Calle for her help with data processing.

Funding

This study was supported by the Fondo de Investigación Sanitaria del Instituto de Salud Carlos III (PI16/188, PI19/855), the European Regional Development Fund (ERDF), and the European Commission through H2020-EU.1.1 and European Research Council grant ERC-2016-StG 715322-EndoMitTalk. This work was partially supported by Comunidad de Madrid (S2017/BMD-3867 RENIM-CM). M.M. is supported by the Miguel Servet Program (CP 19/014). G.S.-H. is supported by FPI-UAM, J.O (FJCI-2017-33855) and E.G-R (IJC2018-036850) by Juan de la Cierva, and E.C. by Atracción de Talento Investigador 2017-T2/BMD-5766 (Comunidad de Madrid and UAM).

Data and materials availability

All data are presented in the main text or the supplementary materials.

Reference and Notes

1. Tarasenko TN, et al. Cytochrome c Oxidase Activity Is a Metabolic Checkpoint that Regulates Cell Fate Decisions During T Cell Activation and Differentiation. Cell metabolism. 2017; 25: 1254–1268. e1257 doi: 10.1016/j.cmet.2017.05.007 [PubMed: 28591633]
2. Weinberg SE, et al. Mitochondrial complex III is essential for suppressive function of regulatory T cells. Nature. 2019; doi: 10.1038/s41586-018-0846-z [PubMed: 30626970]
3. Sena LA, et al. Mitochondria are required for antigen-specific T cell activation through reactive oxygen species signaling. Immunity. 2013; 38: 225–236. DOI: 10.1016/j.immuni.2012.10.020 [PubMed: 23415911]
4. Pearce EL, et al. Enhancing CD8 T-cell memory by modulating fatty acid metabolism. Nature. 2009; 460: 103–107. DOI: 10.1038/nature08097 [PubMed: 19494812]
5. Mills EL, Kelly B, O'Neill LAJ. Mitochondria are the powerhouses of immunity. Nat Immunol. 2017; 18: 488–498. [PubMed: 28418387]

6. Rhoads JP, Major AS, Rathmell JC. Fine tuning of immunometabolism for the treatment of rheumatic diseases. Nat Rev Rheumatol. 2017; 13: 313–320. DOI: 10.1038/nrrheum.2017.54 [PubMed: 28381829]
7. Chang CH, Pearce EL. Emerging concepts of T cell metabolism as a target of immunotherapy. Nat Immunol. 2016; 17: 364–368. DOI: 10.1038/ni.3415 [PubMed: 27002844]
8. Li L, et al. TLR8-Mediated Metabolic Control of Human Treg Function: A Mechanistic Target for Cancer Immunotherapy. Cell metabolism. 2018; doi: 10.1016/j.cmet.2018.09.020 [PubMed: 30344014]
9. Hotamisligil GS. Foundations of Immunometabolism and Implications for Metabolic Health and Disease. Immunity. 2017; 47: 406–420. DOI: 10.1016/j.immuni.2017.08.009 [PubMed: 28930657]
10. Wang A, Luan HH, Medzhitov R. An evolutionary perspective on immunometabolism. Science. 2019; 363 doi: 10.1126/science.aar3932 [PubMed: 30630899]
11. Ron-Harel N, et al. Defective respiration and one-carbon metabolism contribute to impaired naive T cell activation in aged mice. Proc Natl Acad Sci U S A. 2018; 115: 13347–13352. DOI: 10.1073/pnas.1804149115 [PubMed: 30530686]
12. Ekstrand MI, et al. Mitochondrial transcription factor A regulates mtDNA copy number in mammals. Hum Mol Genet. 2004; 13: 935–944. [PubMed: 15016765]
13. Baixauli F, et al. Mitochondrial Respiration Controls Lysosomal Function during Inflammatory T Cell Responses. Cell metabolism. 2015; 22: 485–498. DOI: 10.1016/j.cmet.2015.07.020 [PubMed: 26299452]
14. Ferrucci L, Fabbri E. Inflammageing: chronic inflammation in ageing, cardiovascular disease, and frailty. Nat Rev Cardiol. 2018; 15: 505–522. DOI: 10.1038/s41569-018-0064-2 [PubMed: 30065258]
15. Franceschi C, Garagnani P, Parini P, Giuliani C, Santoro A. Inflammaging: a new immune-metabolic viewpoint for age-related diseases. Nat Rev Endocrinol. 2018; 14: 576–590. [PubMed: 30046148]
16. Furman D, et al. Chronic inflammation in the etiology of disease across the life span. Nat Med. 2019; 25: 1822–1832. DOI: 10.1038/s41591-019-0675-0 [PubMed: 31806905]
17. Chapman NM, et al. mTOR coordinates transcriptional programs and mitochondrial metabolism of activated Treg subsets to protect tissue homeostasis. Nat Commun. 2018; 9 2095 doi: 10.1038/s41467-018-04392-5 [PubMed: 29844370]
18. He S, et al. Gut intraepithelial T cells calibrate metabolism and accelerate cardiovascular disease. Nature. 2019; doi: 10.1038/s41586-018-0849-9 [PubMed: 30700910]
19. Rankin LC, Artis D. Beyond Host Defense: Emerging Functions of the Immune System in Regulating Complex Tissue Physiology. Cell. 2018; 173: 554–567. [PubMed: 29677509]
20. Braumuller H, et al. T-helper-1-cell cytokines drive cancer into senescence. Nature. 2013; 494: 361–365. [PubMed: 23376950]
21. Gomes AP, et al. Declining NAD(+) induces a pseudohypoxic state disrupting nuclear-mitochondrial communication during aging. Cell. 2013; 155: 1624–1638. DOI: 10.1016/j.cell.2013.11.037 [PubMed: 24360282]
22. Verdin E. NAD(+) in aging, metabolism, and neurodegeneration. Science. 2015; 350: 1208–1213. [PubMed: 26785480]
23. Zhang H, et al. NAD(+) repletion improves mitochondrial and stem cell function and enhances life span in mice. Science. 2016; 352: 1436–1443. [PubMed: 27127236]
24. Katsyuba E, et al. De novo NAD(+) synthesis enhances mitochondrial function and improves health. Nature. 2018; 563: 354–359. DOI: 10.1038/s41586-018-0645-6 [PubMed: 30356218]
25. Mitchell SJ, et al. Nicotinamide Improves Aspects of Healthspan, but Not Lifespan, in Mice. Cell metabolism. 2018; 27: 667–676. e664 doi: 10.1016/j.cmet.2018.02.001 [PubMed: 29514072]
26. Elhassan YS, et al. Nicotinamide Riboside Augments the Aged Human Skeletal Muscle NAD(+) Metabolome and Induces Transcriptomic and Anti-inflammatory Signatures. Cell Rep. 2019; 28: 1717–1728. e1716 doi: 10.1016/j.celrep.2019.07.043 [PubMed: 31412242]
27. Bellantuono I. Find drugs that delay many diseases of old age. Nature. 2018; 554: 293–295. [PubMed: 29446384]

28. Lee PP, et al. A critical role for Dnmt1 and DNA methylation in T cell development, function, and survival. Immunity. 2001; 15: 763–774. [PubMed: 11728338]

29. Sawada S, Scarborough JD, Killeen N, Littman DR. A lineage-specific transcriptional silencer regulates CD4 gene expression during T lymphocyte development. Cell. 1994; 77: 917–929. [PubMed: 8004678]

30. Hennet T, Hagen FK, Tabak LA, Marth JD. T-cell-specific deletion of a polypeptide N-acetylgalactosaminyl-transferase gene by site-directed recombination. Proc Natl Acad Sci U S A. 1995; 92: 12070–12074. DOI: 10.1073/pnas.92.26.12070 [PubMed: 8618846]

Europe PMC Funders Author Manuscripts

One Sentence Summary

T cell metabolic stress induces systemic aging.

Europe PMC Funders Author Manuscripts

Europe PMC Funders Author Manuscripts

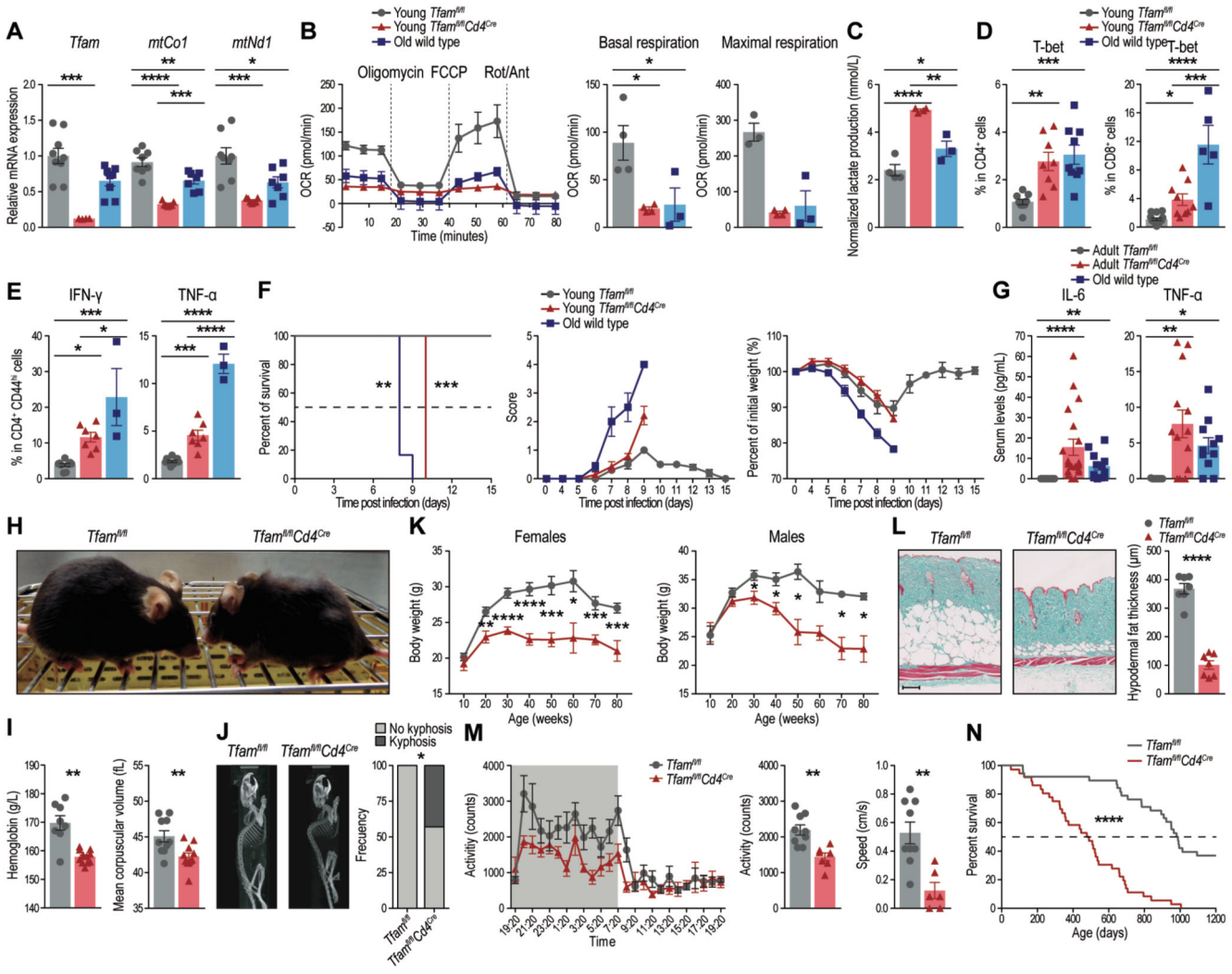

Fig. 1. Mitochondrial dysfunction in T cells causes premature aging.

(**A**) *Tfam, mtCo1* and *mtNd1* mRNA levels in peripheral blood CD4^{+} T cells from young (2-month-old) *Tfam*$^{fl/fl}$ and *Tfam*$^{fl/fl}$ *Cd4*^{Cre} mice, and old (22-month-old) wt mice (n = 6-9 mice per group). (**B**) Oxygen consumption rates (OCR) in activated CD4^{+} T cells from *Tfam*$^{fl/fl}$, *Tfam*$^{fl/fl}$ *Cd4*^{Cre} and old wt animals (left). Basal respiration (center) and maximal respiratory capacity (right) are shown (n = 3-4). (**C**) Lactate content in the supernatant of activated CD4^{+} T cells (n = 3-4). (**D**) Percentages of CD4^{+} (left) and CD8+ (right) T cells positive for the Th1 cell transcription factor T-bet (n = 5-14). (**E**) Percentages of CD4+CD44^{hi} T cells staining positive for intracellular IFN-γ and TNF-α (n = 3-9). (**F**) Post-infection survival curves (left panel) for *Tfam*$^{fl/fl}$, *Tfam*$^{fl/fl}$ *Cd4*^{Cre} and old wt mice inoculated s.c. with ECTV (10^{3} PFUs per mouse). ECTV-infected mice were monitored daily for clinical signs of illness (center) and change from initial body weight (right). Signs of illness are expressed as means ± SEM using an individual score ranging from 0 for healthy animals to 4 for severely diseased animals (n = 5-7). (**G**) Serum levels of inflammatory cytokines IL-6 and TNF-α detected by Multiplex in 7-month-old *Tfam*$^{fl/fl}$ and *Tfam*$^{fl/fl}$ *Cd4*^{Cre} mice and 22-month-old wt mice (n = 10-19). (**H**) Representative

photograph showing the deteriorated physical appearance of a *Tfam*$^{fl/fl}$ *Cd4*^{Cre} mouse (right) compared with a control littermate (left), both aged 7 months. (**I**) Hematological parameters in *Tfam*$^{fl/fl}$ *Cd4*^{Cre} and *Tfam*$^{fl/fl}$ mice (n = 8-11, 5 months old). (**J**) Quantification of spine curvature by computed tomography (CT) scans (left) and percentage of mice presenting lordokyphosis (right) in 5-month-old *Tfam*$^{fl/fl}$ *Cd4*^{Cre} mice (n = 7-8). (**K**) Body weight evolution in *Tfam*$^{fl/fl}$ and *Tfam*$^{fl/fl}$ *Cd4*^{Cre} female (left) and male (right) mice (n = 8-20). (**L**) Representative skin sections stained with Masson trichrome (left) and quantification of hypodermal fat thickness (right). At least 10 measurements were performed per animal. The graph shows mean values for n = 7, 7 months of age. Scale bar: 100 μm. (**M**) Activity time course over a 24-hour cycle (left) and mean dark period activity (center) and speed (right) assessed in metabolic cages (n = 6-9, 7-month-old mice). Bar graphs correspond to the dark (active) period. (**N**) Kaplan-Meier survival curves for *Tfam*$^{fl/fl}$ and *Tfam*$^{fl/fl}$ *Cd4*^{Cre} mice (n = 36-38, including males and females). Dots in all panels represent individual sample data. Data are presented as means ± SEM. Statistical analysis was by one-way analysis of variance (ANOVA) with post hoc Tukey's correction [**A** (*mtCo1* and *mtNd1*), **C**, **D** and **G** (TNF-α)]; Kruskal–Wallis *H* test with post hoc Dunn's correction [**A** (*Tfam*), **B** and **G** (IL-6)], unpaired Student's t-test [**I** (MCV), **J, K** and **M**]; or unpaired Welch's t-test [**L** and **I** (Hemoglobin)]. *p<0.05, **p<0.01, ***p<0.001, ****p<0.0001. Survival curve data were analyzed by log-rank (Mantel-Cox test) [**F** and **N**]. For the ECTV experiment, data correspond to one representative experiment of two.

Europe PMC Funders Author Manuscripts

Europe PMC Funders Author Manuscripts

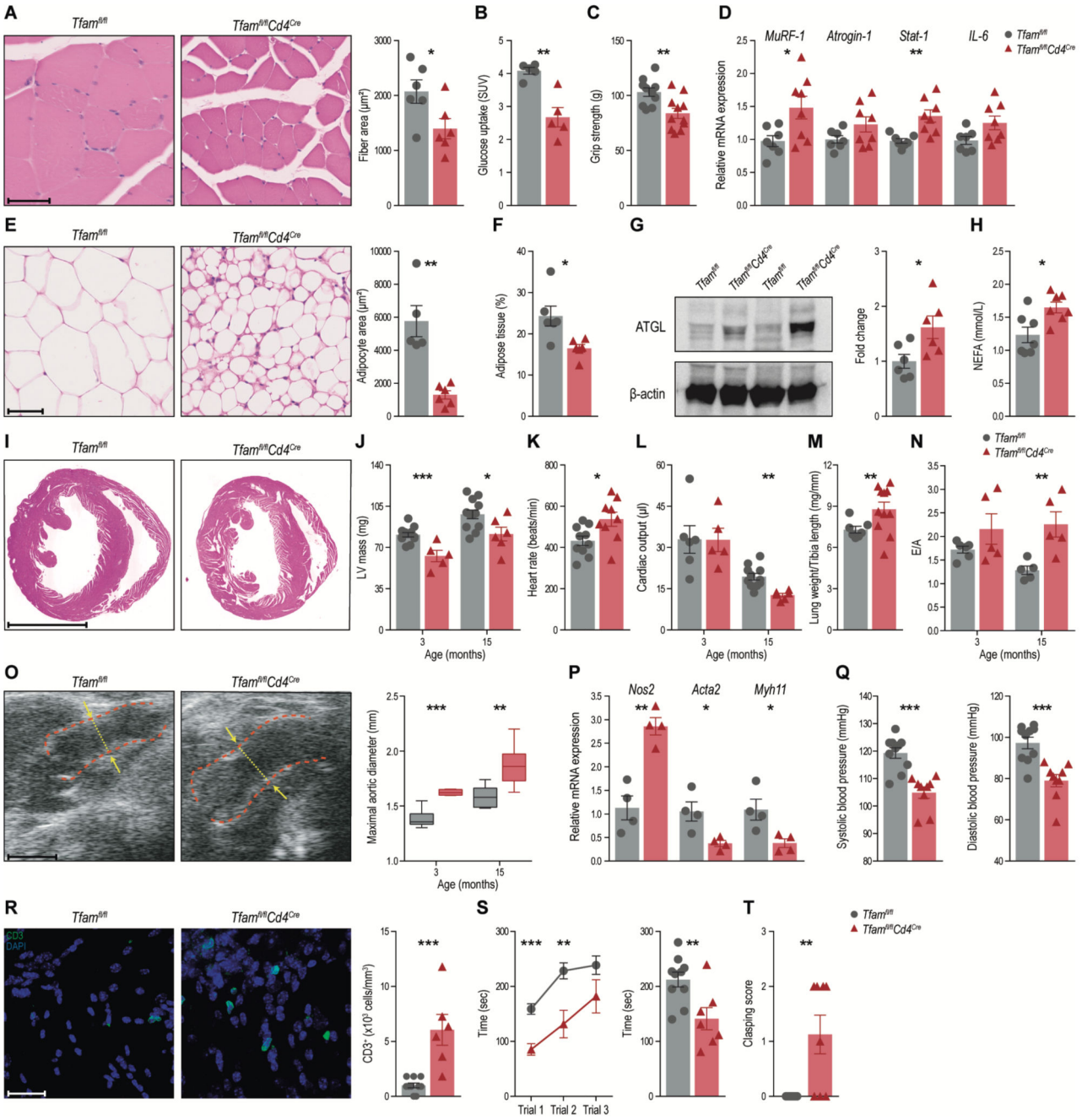

Fig. 2. *Tfam*$^{fl/fl}$ *Cd4*^{Cre} mice develop age-associated multimorbidity.

(**A**) Representative haematoxylin and eosin (H&E)-stained sections of gastrocnemius muscle (left, scale bar: 50 µm) and quantification of myofiber cross-sectional area (right). At least 10 measurements were performed per animal. The graph shows mean fiber area for n = 6 animals per group (7-month-old mice). (**B**) In vivo positron emission tomography and computed tomography analysis of skeletal muscle glucose uptake. Data are mean ± SEM of ^{18}F-FDG activity (n = 5, 4-month-old mice). SUV, standard uptake. (**C**) Forelimb grip strength analysis (n = 10-11, 7-month-old mice). (**D**) Relative mRNA levels of genes related

to muscle proteolysis (*MuRF*-1 and *Atrogin*-1) and inflammation (*Stat1* and *IL-6*) (n = 7-8, 7-month-old mice). (**E**) Representative H&E stained sections of gWAT from $Tfam^{fl/fl}$ $Cd4^{Cre}$ and $Tfam^{fl/fl}$ mice (left, scale bar: 50 μm). The graph (right) shows mean estimated adipocyte surface area. Ten measurements were performed per animal (n = 5-6 animals, 7-month-old mice). (**F**) Percentage of adipose tissue determined by quantitative magnetic resonance imaging in $Tfam^{fl/fl}$ $Cd4^{Cre}$ and $Tfam^{fl/fl}$ mice (n = 6, 7-month-old mice). (**G**) Immunoblot (left) and densitometry analysis (right) of ATGL protein expression in gWAT isolated from $Tfam^{fl/fl}$ $CD4^{Cre}$ mice and control littermates (n = 6, 7-month-old mice). (**H**) Plasma non-esterified fatty acids (NEFA) (n = 7, 4-month-old mice). (**I**) Representative H&E-stained heart sections from 15-month-old $Tfam^{fl/fl}$ $Cd4^{Cre}$ and $Tfam^{fl/fl}$ mice. Scale bar: 2.5 mm (**J**) Echocardiography measurements of left ventricular (LV) mass in 3- and 15-month-old $Tfam^{fl/fl}$ and $Tfam^{fl/fl}$ $Cd4^{Cre}$ mice (n = 5-12). (**K**) Heart rate in 3-month-old $Tfam^{fl/fl}$ $Cd4^{Cre}$ mice and control littermates (n = 9-10). (**L**) Cardiac output in 3- and 15-month-old $Tfam^{fl/fl}$ and $Tfam^{fl/fl}$ $Cd4^{Cre}$ mice (n = 5-11). (**M**) Lung weight normalized to tibia length in $Tfam^{fl/fl}$ and $Tfam^{fl/fl}$ $Cd4^{Cre}$ mice (n = 7-11, 7-month-old mice). (**N**) Mitral flow pattern on echocardiography in 3- and 15-month-old $Tfam^{fl/fl}$ and $Tfam^{fl/fl}$ $Cd4^{Cre}$ mice (n = 5-6). (**O**) Representative ultrasound images depicting maximal ascending aorta diameters in 15-month-old $Tfam^{fl/fl}$ and $Tfam^{fl/fl}$ $Cd4^{Cre}$ mice (left, scale bar: 1 mm) and quantification of maximal aortic diameter in 3- and 15-month-old $Tfam^{fl/fl}$ and $Tfam^{fl/fl}$ $Cd4^{Cre}$ mice (right) (n = 6-8). Maximal aortic diameter is presented in box-and-whisker plots showing maximal and minimal values and 75th and 25th percentiles. (**P**) RT-qPCR analysis of *Nos2, Acta2*, and *Myh11* mRNA expression levels in aortic samples from 7-month-old $Tfam^{fl/fl}$ and $Tfam^{fl/fl}$ $Cd4^{Cre}$ mice (n = 4). (**Q**) Systolic and diastolic blood pressure in 3-month-old $Tfam^{fl/fl}$ and $Tfam^{fl/fl}$ $Cd4^{Cre}$ mice (n = 9-10). (**R**) Representative CD3-stained brain (*fornix*) sections from 15-month-old $Tfam^{fl/fl}$ and $Tfam^{fl/fl}$ $Cd4^{Cre}$ mice (scale bar: 25 μm) and quantification of CD3 positive cell density (n = 6-10). (**S**) Rotarod test performance by $Tfam^{fl/fl}$ and $Tfam^{fl/fl}$ $Cd4^{Cre}$ mice, expressed as the mean time spent on the rotating rod in each of three trials (left) and all trials combined (right) (n = 7-10, 12-month-old mice). (**T**) Maximum clasping score per 30 s test (n = 8-9, 12-month-old mice). Dots in all panels represent individual sample data. Data are presented as means ± SEM. Box plots represent the median and the 25th and 75th percentiles. Statistical analysis was by unpaired Student's *t*-test [**A** to **C, D** (*MuRF-1, Atrogin, IL-6*), **F** to **L, N** and **O** (15mo), **P, Q** (Diastolic pressure) and **S**]; unpaired Welch's *t*-test [**D** (*Stat1*), **M** and **N** and **O** (3mo)]; or nonparametric Mann–Whitney *U* test [**Q** (Systolic pressure), **R** and **T**]. *p<0.05, **p<0.01, ***p<0.001, ****p<0.0001.

Europe PMC Funders Author Manuscripts

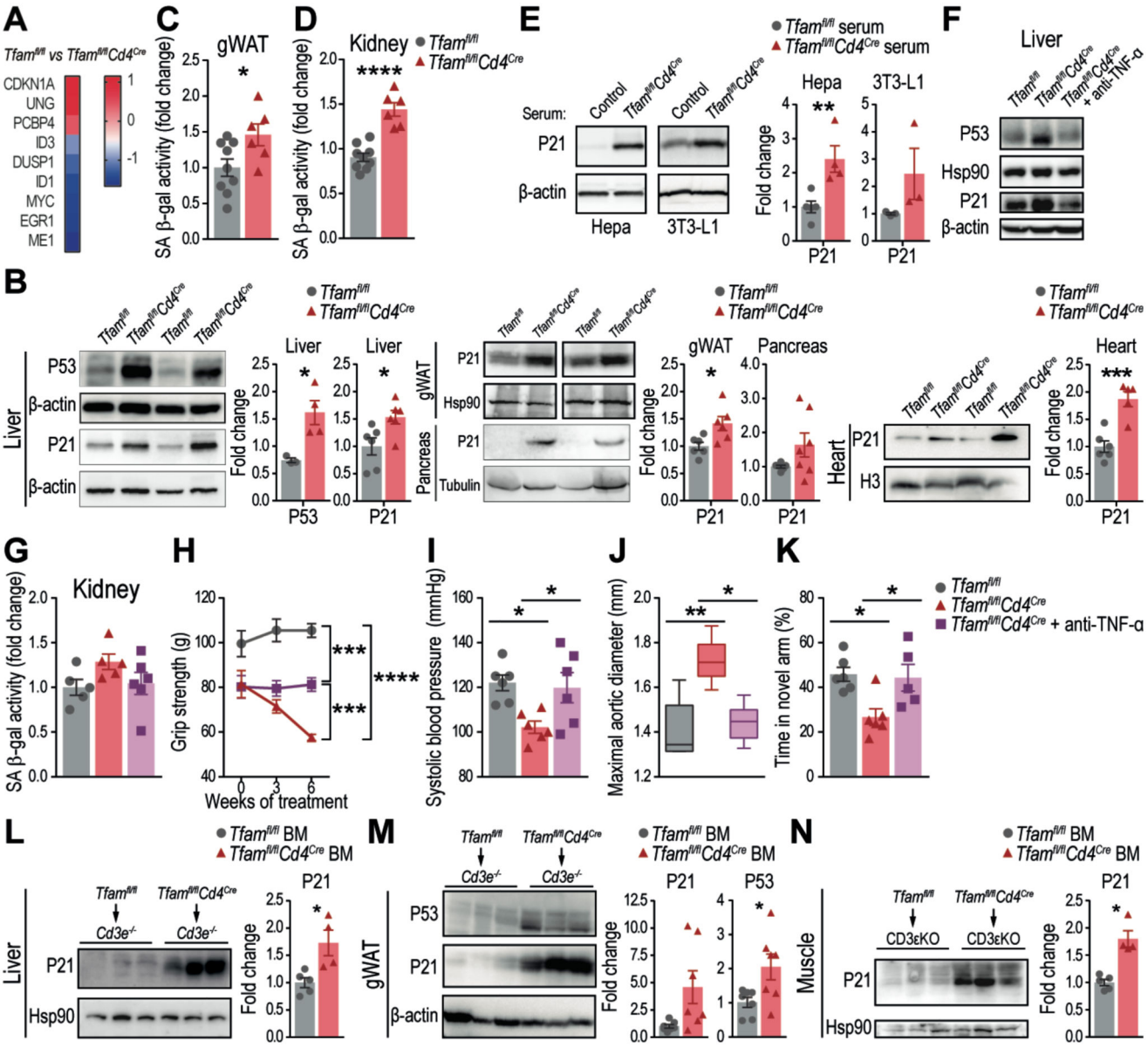

Fig. 3. Inflammaging induces senescence in distal tissues of *Tfam*$^{fl/fl}$ *Cd4*^{Cre} mice.

(**A**) Heatmap of senescence gene expression changes comparing liver from *Tfam*$^{fl/fl}$ *Cd4*^{Cre} mice and control littermates. (**B**) Representative immunoblot (left) and quantification (right) of p21 and p53 protein expression in liver, heart, gWAT, and pancreas from *Tfam*$^{fl/fl}$ *Cd4*^{Cre} and *Tfam*$^{fl/fl}$ mice. Loading controls were β-actin, H3, Hsp90 or α-tubulin (n = 4-7, 7-month-old mice) (**C**) Quantitative measurements of β-galactosidase activity in gWAT lysates by colorimetric assay (n = 6-9, 9-month-old mice). (**D**) Quantitative measurements of β-galactosidase activity in kidney lysates by colorimetric assay (n = 6-9, 12-month-old mice). (**E**) Immunoblot (left) and densitometry analysis (right) of p21 expression in immortalized mouse hepatocytes and 3T3-L1 cells cultured for 7 days in the presence of *Tfam*$^{fl/fl}$ or *Tfam*$^{fl/fl}$ *Cd4*^{Cre} serum from 7-month-old mice. β-actin was used as a loading control (n

= 4-6). Blots are representative of three (3T3-L1) or four (hepatocytes) experiments using pooled sera from three animals. (**F**) Representative immunoblot analysis of senescence markers in liver from control *Tfam*$^{fl/fl}$ and *Tfam*$^{fl/fl}$ *Cd4*^{Cre} mice with or without treatment with anti-TNF-α (etanercept) (n = 6, 10 weeks of treatment starting from 4 months of age). (**G**) β-galactosidase activity measured by a colorimetric assay in kidney lysates (n = 6, 10 weeks of treatment). **(H)** Time course of forelimb strength during anti-TNF-α treatment. (**I**) Systolic blood pressure after 7 weeks of anti-TNF-α treatment (n = 6). (**J**) Maximal ascending aorta diameter in response to anti-TNF-α treatment (n = 6, 8 weeks of treatment). Maximal aortic diameter is presented in a box-and-whisker plots showing maximal and minimal values and 75th and 25th percentiles. (**K**) Y-Maze analysis in *Tfam*$^{fl/fl}$ *Cd4*^{Cre} mice treated with anti-TNF-α and corresponding controls (n = 6, 8 weeks of treatment). (**L-N**) Immunoblot (left) and densitometry analysis (right) of p21 or p53 expression in liver (**L**), gWAT (**M**), and tibialis muscle (**N**) from *Cd3e*$^{-/-}$ mice 16 weeks after reconstitution with bone marrow from *Tfam*$^{fl/fl}$ *Cd4*^{Cre} or *Tfam*$^{fl/fl}$ mice (n = 4-6 per group). Dots in all panels represent individual sample data. Data are presented as mean ± SEM. Statistical analysis was by one-way analysis of variance (ANOVA) with post hoc Tukey's correction [**G, I** and **K**]; Kruskal–Wallis test with post hoc Dunn's correction [**J**]; two-way ANOVA with post hoc Tukey's correction [**H**]; unpaired Student's *t*-test [**B, C, D, E, L** and **M**] or nonparametric Mann–Whitney *U* test [**N**]. *p<0.05, **p<0.01, ***p<0.001, ****p<0.0001.

Europe PMC Funders Author Manuscripts

Europe PMC Funders Author Manuscripts

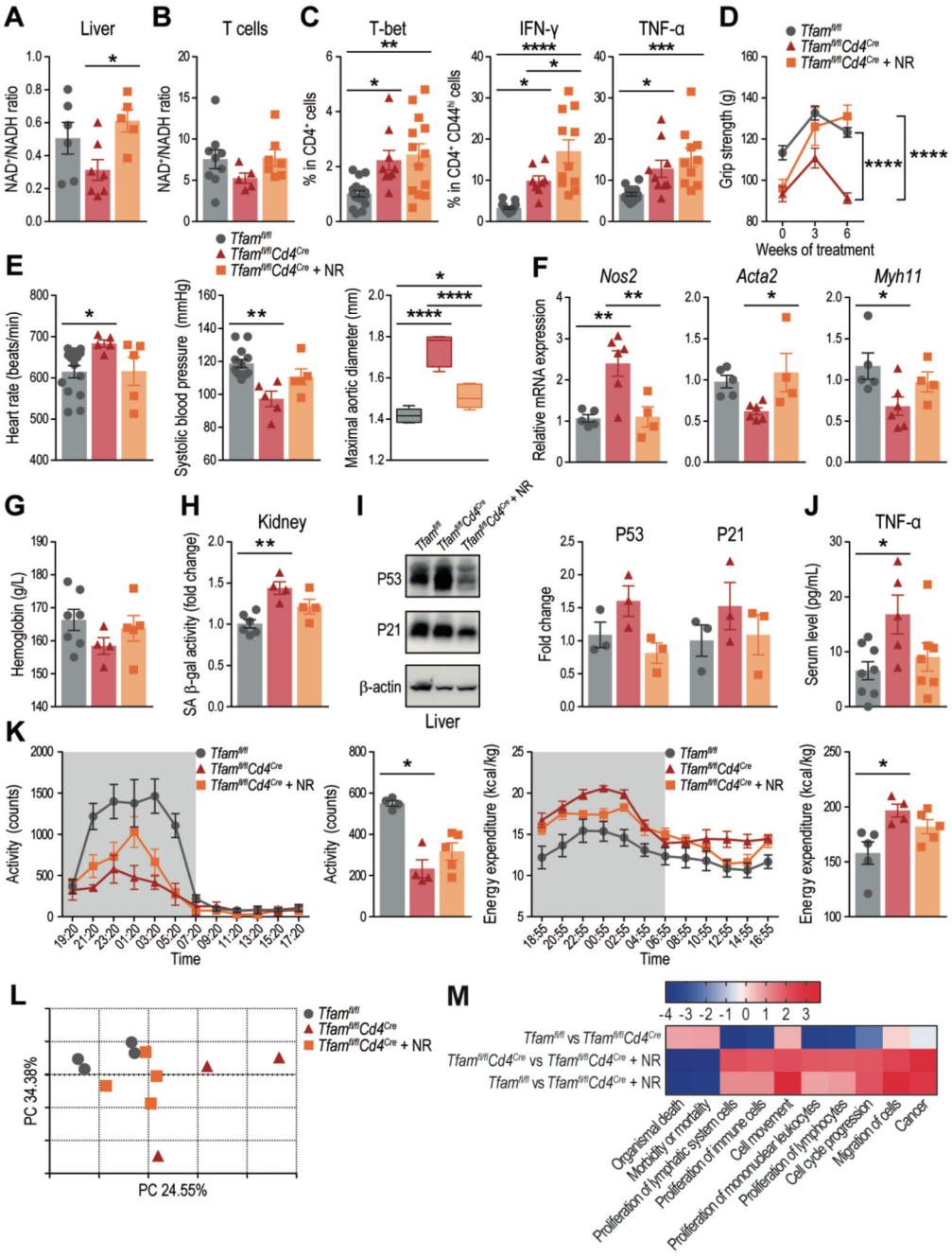

Fig. 4. Nicotinamide riboside (NR) treatment rescues the multimorbidity syndrome.

(**A, B**) NAD^+/NADH ratio in liver (A) and in isolated $CD4^+$ T cells (B) lysates from untreated *Tfam*$^{fl/fl}$, *Tfam*$^{fl/fl}$ *Cd4*^{Cre}, and NR-treated *Tfam*$^{fl/fl}$ *Cd4*^{Cre} mice (n = 5-9 per group, 10-week treatment starting from 4 months of age). (**C**) FACS analysis of intracellular T-bet (left), IFN-γ (center) and TNF-α (right) in splenic $CD4^+$ T cells (n = 8-17). (**D**) Effect of NR treatment on the evolution of forelimb strength (n = 5-11). (**E**) Heart rate (left), systolic blood pressure (center), and ascending aorta (AsAo) maximum diameter (right) obtained from ultrasound images after 8 weeks of NR treatment. Maximal aortic

diameter is presented in a box-and-whisker plot showing the median and the 25th and 75th percentiles (n = 5-14). (**F**) RT-qPCR analysis of *Nos2, Acta2*, and *Myh11* mRNA expression in aorta from untreated $Tfam^{fl/fl}$, $Tfam^{fl/fl}$ $Cd4^{Cre}$ and, NR-treated $Tfam^{fl/fl}$ $Cd4^{Cre}$ mice (n = 4-6). (**G**) Blood hemoglobin levels (n = 4-7). (**H**) β-galactosidase activity measured by colorimetric assay in kidney lysates (n = 4-6). (**I**) Western blot (left) and densitometry analysis (right) of p21 and p53 expression in liver lysates from untreated $Tfam^{fl/fl}$, $Tfam^{fl/fl}$ $Cd4^{Cre}$ and $Tfam^{fl/fl}$ $Cd4^{Cre}$ mice treated with NR for 10 weeks (n = 3-4). β-actin was used as a loading control. (**J**) Circulating TNF-α determined by Multiplex analysis in serum from untreated $Tfam^{fl/fl}$, $Tfam^{fl/fl}$ $Cd4^{Cre}$, and NR-treated $Tfam^{fl/fl}$ $Cd4^{Cre}$ mice (n = 5-8). (**K**) Activity (left) and energy expenditure (right) monitored over a 24-hour cycle in metabolic cages (n = 4-5). (**L**) Principal component (PC) analysis of transcriptomics in liver samples from untreated $Tfam^{fl/fl}$, $Tfam^{fl/fl}$ $Cd4^{Cre}$ and $Tfam^{fl/fl}$ $Cd4^{Cre}$ mice treated with NR for 10 weeks (n = 3-4). (**M**) IPA heatmap showing transcriptionally altered cellular pathways. Dots in all panels represent individual sample data. Data are presented as mean ± SEM. Statistical analysis was by one-way analysis of variance (ANOVA) with post hoc Tuley's correction [**A** to **C, E** (Maximal aortic diameter), **G, H, I** (p21), **J and K** (Energy expenditure)]; Kruskal-Wallis *H* test with post hoc Dunn's correction [**E** (Heart rate and Systolic blood pressure), **F, I** (p53) and **K** (Activity)]; or two-way ANOVA with correction post hoc Tukey's correction [**D**]. *p<0.05, **p<0.01, ***p<0.001, ****p<0.0001.